
Article:
Serrazina, R., Dean, J.S. orcid.org/0000-0001-7234-1822, Reaney, I.M. orcid.org/0000-0003-3893-6544 et al. (3 more authors) (2019) Mechanism of densification in low-temperature FLASH sintered lead free Potassium Sodium Niobate (KNN) piezoelectrics. Journal of Materials Chemistry C. ISSN 2050-7526

https://doi.org/10.1039/c9tc03117k

(Revised version of paper submitted to Journal of Materials Chemistry C, # TC-ART-06-2019-003117, 06 Oct 2019)

Mechanism of densification in low-temperature FLASH sintered lead free Potassium Sodium Niobate (KNN) piezoelectrics

Ricardo Serrazina[1], Julian S. Dean[2], Ian M. Reaney[2], Luis Pereira[3], Paula M. Vilarinho[1*], Ana M. O. R. Senos[1]

[1] Department of Materials and Ceramic Engineering, CICECO – Aveiro Materials Institute, University of Aveiro, 3810-193 Campus Santiago, Portugal
[2] Materials Science and Engineering, University of Sheffield, Sheffield S1 3JD, UK.
[3] Materials Science Department, CENIMAT-I3N, Faculty of Science and Technology, University NOVA de Lisboa, Campus da Caparica. 2829-516 Caparica, Portugal

*Corresponding author: paula.vilarinho@ua.pt

Abstract

Lead-free potassium sodium niobate ($K_{0.5}Na_{0.5}NbO_3$, KNN) piezoelectric ceramics have been densified at temperatures lower than 300 ºC using atmosphere-water assisted FLASH sintering. Transmission electron microscopy (TEM) studies revealed amorphous phase at grain boundaries that resulted from surface melting of the cuboid particles in the presence of segregated impurities. We propose that preferential surface melting of the primary particles is induced in conductive channels of open pores in which water is adsorbed. This creates a network of pathways for the

electric current. The resulting liquid phase induces fast densification through sliding of grain boundaries and viscous flow of the liquid driven by minimisation of surface energy. Finite Element Modelling (FEM) revealed that current density and Joule heating were also influenced by the geometry of contact between the cuboid KNN particles with vertex to vertex inducing the maximum current density and consequently creating the greatest volume of amorphous phase in adjacent pores. The lowest current density was predicted for face to face contacts, resulting in only a thin amorphous layer between grains.

Key words: cleaner synthesis technology, sustainable sintering, lead-free piezoceramics, FLASH, low temperature sintering, potassium sodium niobate, $K_{0.5}Na_{0.5}NbO_3$ (KNN), Finite Element Modelling (FEM), transmission electron microscopy (TEM).

Introduction

Reduction in CO_2 emissions during the fabrication and densification of ceramics is particularly important as this industry consumes a disproportionate amount of energy in comparison to the size of the sector [1]. Ferroelectrics are an important class of ceramics that find applications in sensors and actuators, critical for the development of Industry 4.0 and Internet of Things [2]. However, such materials are sintered commercially at > 1000 ºC for several hours.

As an alternative to such high energy consumption processes, FLASH sintering was proposed [3]. FLASH is a field-assisted, very fast, low-temperature, sintering

technique, in which the specimen is placed between electrodes with densification occurring in a few seconds (≤ 60 s) during a limited current controlled stage [4], [5]. With the use of specific atmospheres and water, as well as electric field/current conditions, FLASH sintering temperature and time can be significantly decreased from around 1000 ºC for several hours towards room temperature for a few seconds [6]. Reducing densification time and temperature can also minimise the loss of volatile components, potentially maintaining stoichiometry and improving the performance of compounds such as $(K_{1-x}Na_x)NbO_3$ (KNN). [7]

KNN is a potential PbO free substitute for $Pb_{1-x}Zr_xTiO_3$ (PZT), currently the market leader for piezoelectric actuators, sensors, and transducers [8]. Undoped monophasic $K_{0.5}Na_{0.5}NbO_3$ has a high Curie temperature ($T_C \approx 420$ °C), a piezoelectric coefficient d_{33} between 80 to 160 pC/N and an electromechanical coupling coefficient k_P of 0.39. [9]. However, undoped KNN is conventionally sintered at 1100 ºC for more than 1 h [10] which induces volatilization of K and Na, triggering the formation of secondary phases that affect properties. Sintering lead-free KNN at lower times and/or temperatures would alleviate these issues as well as making its production more energy efficient, contributing to sustainability. FLASH sintered KNN has previously been reported to achieve 94% density at 990 ºC, 250 $V.cm^{-1}$ and 20 $mA.mm^{-2}$ for 30 s [11]. However, the road map towards a sustainable ceramics manufacturing demands drastic decreases in temperature and time and it is debateable whether a reduction of ~100 ºC is enough to warrant the cost of retooling production to utilise FLASH sintering.

In a general way, three mechanisms are proposed to explain FLASH: (i) Joule heating, (ii) field induced defects and (iii) changes of interfacial energy. These should not be described as individuals, because they all influence the process. Generally,

sintering is highly dependent on the diffusion rate at grain boundaries. The electric field enhances this diffusion. During FLASH a current would pass through the sample, which increases its temperature by Joule heating. At low temperature, the amount of heat is negligible, since the current is low. However, the resistance of ceramics decreases with increasing temperature.

Furthermore, two separated studies [12], [13] suggest that the ultrahigh heating rate generated during FLASH is a critical factor that lead to fast densification by (i) preventing the initial coarsening, keeping a high densification driving force, as already explained, and (ii) providing non-equilibrium defects that would enhance matter flow. Those defects can be, for instance, grain boundary structures (or complexions [14], [15]) with enhanced mass transport rates [16], or Frenkel pairs nucleation [17]–[19]. All the described factors increase the diffusion rate at grain boundaries (i.e. particle surfaces) and, consequently, enhance the densification rate [20].

Recently, it was shown that, for YSZ, the FLASH sintering mechanism is controlled by the electric current limit; if a critical current threshold is exceeded ($J > 10$ $mA.mm^{-2}$), alternative densification mechanisms are activated. On the other hand, for low current density (5 $mA.mm^{-2}$) the densification mechanism is similar to an accelerated conventional sintering [21].

Regarding FLASH mechanisms, and as pointed out by Dancer [5], there are currently several contradictions in the community. FLASH sintering seems to be a material dependent process and general mechanism description is not easy to attain. Also, specific studies on the mechanism of FLASH sintering of complex oxides are mandatory to further understand the general phenomena but also the particularities of specific systems.

A limited number of efforts have been made to model FLASH phenomena. Furthermore, few works on modelling Joule heating have been published. The electric field distribution has been modelled for a dog-bone shape specimen [22]. Also, Naik and co-workers [23] proposed a model for the nucleation of defects under an electric field for isothermally FLASH sintered 3YSZ-Al_2O_3; the model shows that the Joule heating is a consequence of nucleation of defects and not the cause of it [23].

In this work, we conduct a systematic analysis of the GBs of low temperature (< 300 ºC) water assisted FLASH sintered KNN ceramics; we support our observations with Finite Element Modelling (FEM) to estimate local Joule heating, considering the geometry of particle to particle contact. ZnO has already been FLASH sintered at room temperature [6] using similar conditions to those reported here, however, KNN is a complex, ternary oxide, with potential applications as a lead free piezoelectric and thus, this work has far reaching consequences for the potential commercial usage of water assisted FLASH sintering to reduce carbon emissions within the ceramic sector.

Experimental

$K_{0.5}Na_{0.5}NbO_3$ powders were prepared by a conventional solid-state route. High purity carbonates (K_2CO_3, Merck, 99.0% and Na_2CO_3, Chempur, 99.5%) and niobium oxide (Nb_2O_5, Alfa Aesar, 99.9%) were mixed in teflon jars, with YSZ and ethanol media, at 200 RPM for 6 h. A calcination step at 900 ºC, for 3 h, was performed. The final milling step was for 27 h, using the same initial milling conditions.

Particle size distribution was assessed by laser particle diffraction (COULTER LS-200), in which two maxima were identified: at 200 nm and at 1.7 μm. More than 75% of the particle size distribution was below 445 nm. The largest registered particle size was 4 μm.

FLASH experiments were conducted with parallelepiped shape specimens on samples with 65 $\pm$ 3 % green density, which were shaped by uniaxial and isostatic pressing, at 130 MPa for 90 s and 350 MPa for 15 min, respectively.

FLASH sintering was performed in an alumina tube furnace using a setup as represented in Figure 2. One fixed alumina part and platinum electrode were placed in one side of the setup. A movable alumina rod, which pushes the second Pt electrode, was placed in the opposite side. An external spring allows the system to maintain electrode contact during the specimen shrinkage. Two platinum wires were connected to the platinum electrodes and to the power source (DC, EPS HV 5006-400).

A mixture of gas and water was utilised following procedures described by ref. [6] by flowing argon through a flask of deionized water, allowing to perform the densification of KNN at temperatures as low as 290 ºC. The FLASH setup was purged for 1 h with the Ar + H_2O mix at approximately 500 ml.min^{-1}. After purging, a DC electric field was applied (400 V.cm^{-1}) and temperature increased at a rate of 10 ºC.min^{-1}. The current was limited to 60 mA.mm^{-2} and the gas flux was kept constant. Heating was stopped immediately after FLASH occurred. The FLASH time, defined as the time in current limit control, was 60 s.

Figure 2 shows the x-ray pattern for powders and FLASH sintered KNN indexed with PDF file 01-084-6855. The data was collected with a PANalytical XPERT-PRO diffractometer. Despite that no secondary phases were observed in the FLASH sintered body, a decrease in peak definition and sharpness is observed, which can be indicative of partial grain amorphization. This observation justified the electron microscopy and modelling studies presented in this work.

Scanning electron microscopy (SEM, HITACHI S-4100) and Transmission electron microscopy (TEM, JEOL JEM 2200 FS) with Energy-dispersive X-ray spectroscopy (OXFORD Inca x-sight) were used to systematically analyse the microstructure of FLASH sintered KNN and, specifically, grain boundaries. For TEM experiments, the sintered specimens were polished using the tripod method, with diamond lapping paper. The polished specimens were attached to a molybdenum ring and ion milled with a GATAN PIPS.

Finite element modelling (FEM) presented here used the ANSYS® Academic Research Mechanical, Release 18.1 package. Simulations were performed using electrical analysis in order to study current density, electric field and associated Joule heating effects arising from the microstructure. An adaptive refinement, dividing the mesh length by approximately 1/3rd, were implemented around the connection points to account for the extra complexity in the solution. To reach convergence in the models a mesh size of 25 nm was used, generating over 1 million tetrahedral elements. It is important to highlight that FEM work is developed considering a stationary system in which electrical properties of the material do not change with the application of the field. We note that the goal of our study is to understand the role of contact geometry rather than attempt a full FEM analysis of field distributions in FLASH sintering.

Results and Discussion

Figure 3a shows a uniaxial and isostatically pressed green pellet cross section with figure 3b an equivalent image of FLASH sintered KNN. The green pellet (figure 3a) is composed of randomly distributed cuboid particles with coarser particles ~4 μm; and fine particles < 0.5 μm, in accordance with PSD analysis. Figure 3b) reveals that the coarser particles did not grow during sintering and that the finer particles are less

evident. Low magnification SEM images (figure 3c)) also reveal that the densest regions occur in channels throughout the specimen, indicating that electric field and current are non-uniformly distributed.

The overall densification of the atmosphere-water assisted FLASH sintered KNN under the conditions here reported is approximately 80 % of theoretical densification. However, and as specifically shown in figure 3 c), densification is not homogeneous. Figure 3 b) highlights the comparison between very high dense areas and some porous ones. In some regions densification as high as 100%, can be achieved. This phenomenon (well known for FLASH sintering) is due to the current channeling that happens during the FLASH process and as a consequence the densification of the sample is not uniform. We attribute this to current and densification pathways to open pores in which the water vapour from the furnace atmosphere has adsorbed onto the surface of the particles. We also note the absence of defined grains in the densest regions (figure 3b), potentially indicating partial melting.

A representative TEM micrograph of FLASH sintered KNN is shown in figure 4. Consolidation of primary particles was evident, confirming the SEM results. Moreover, an amorphous phase is present at most GBs, irrespective of the contact geometry. The amorphous phase was identified through the absence of discrete diffraction spots in electron diffraction patterns. In addition, we note that conventionally sintered KNN TEM samples fabricated under identical ion beam milling conditions do not exhibit amorphization. We conclude therefore, that the amorphous phase is not an artefact of TEM sample preparation.

In some cases, penetration of one grain into its neighbor grain is apparent, as illustrated by the arrows in figure 4. Furthermore, no grain growth is observed, and coarser grains remain < 4 μm. These observations suggest that mass transport

through conventional diffusion is not the dominant sintering mechanism in water assisted FLASH KNN. Our observations contradict previous reports of grain growth of KNN after 30 s of FLASH in air and at 250 $V.cm^{-1}$, 20 $mA.mm^{-2}$ [11]. Several parameters may contribute to these discrepancies such as the use of different atmosphere, electrical current limit, specimen shape and primary particle size. However, our observations suggest that water assisted FLASH promotes the formation of a liquid phase in KNN which appears as amorphous material within intergranular pores on cooling, circled in figure 4. There is no evidence of a similar amorphous phase in conventionally sintered samples [24]. Our observations are therefore, broadly in agreement with Narayan [25], [26] who predicted local melting through a high current density at GBs. As pointed out by Dancer [5], Narayan's model requires that FLASH occurs in the presence of a liquid phase, and it would be expected that some evidence of that high temperature viscous phase would be present at the GBs [10], [27]. Moreover, R. Chaim and co-works showed that particle surface softening by liquid film formation during FLASH contributes considerably to the fast sintering process. Furthermore, they have shown that thermal gradient between the solid particle and its melted/softened surface can be as high as 3000 K [28], [29].

Our TEM studies further suggest that conventional mass transport via diffusion is limited and that a more likely explanation is densification through minimisation of surface energy facilitated by the sliding of grains within a viscous liquid medium. Therefore, we suggest that water assisted FLASH sintering in KNN occurs mainly through channelling of current through open pores, which have adsorbed water on the surface of the particles. Given this proposed mechanism, the anisotropy of KNN primary particles (cuboid) might also be expected to influence current density distribution, the Joule heating, local temperature and thus the extent of formation of a

liquid phase (volume of residual amorphous material on cooling). There are four potential arrangements of cuboid contact in the green body prior to FLASH: (i) face-face, both in (100) direction; (ii) edge-face, (100) with (110) direction, (iii) vertex-face, direction (111) with (100); and (iii) vertex with vertex, both in (111) direction.

Based on simplistic field enhancement, the current density is expected to be higher in geometries with the lowest contact area and this should then be reflected in the volume of amorphous phase in adjacent regions. Figure 5 exemplifies the face-face contact direction. The current and Joule heating runaway induces the grain boundaries melting and sliding, resulting in the observed consolidation. The inset in figure 5 is a magnified image which shows more clearly the thin amorphous layer at the GB.

At a vertex-face boundary, the melting and volume fraction of amorphous phase should be more pronounced. Figure 6 shows a region where there is contact of the central grain via the vertex to the faces of adjacent grains. Evidence of local melting is observed through the interpenetration of the vertices with the faces (outlined) and through the amorphous phase which is contained in the intergranular pore (arrowed). Note that the amorphous phase appears to ion thin more quickly than the KNN grains, as illustrated by its lacey appearance. It is likely that the entire pore was filled with amorphous phase in the bulk ceramic prior to thinning. This interpretation is supported by the SEM image of the FLASH sintered ceramic in figure 3, in which individual grains are difficult to distinguish in some parts of the image and are likely surrounded by amorphous phase.

Figure 7 (a) adds further microstructural evidence to GB melting driven by local Joule heating. This unusual microstructure is atypical of conventional sintered KNN grain boundaries and is interpreted as a relic microstructure formed by the outward

diffusion of ions to the particle surface. The amorphous phase is present at the GB and the tree root shape of grain boundary amorphization may be a consequence of thermal gradient [28]. Furthermore, representative diffraction patterns (TEM JEOL H-9000, at 300 kV) of the amorphous areas and grains are also shown in figure 7 (b) and (c), respectively. These patterns account for the clear perovskite crystalline structure of the grains (with a 110 zone axis), and a non-crystalline evidence of the designated amorphous areas (scattered rings). Such observation confirms what is suggested by the TEM image interpretation, which is the clear amorphization of grain boundaries and filling of pores with such amorphous phase.

To determine the approximate chemical composition of the amorphous region resulting from liquid phase formed during water assisted FLASH, energy-dispersive X-ray spectroscopy (EDS) was performed. The EDS results are presented in figure 8. Such analysis indicates that the chemical composition of the bulk of grains after FLASH is close to stoichiometric, which was expected from the structural analysis provided by TEM diffraction patterns (figure 7 (c)). In contrast, the amorphous phase is Na deficient and Nb and Al rich. Al_2O_3 is not a constituent of KNN but is present as impurities through raw materials and as a result of milling. We propose that during FLASH sintering Al segregates to the GBs and participates in the formation of a liquid phase; simultaneously Na is volatilised [23] leaving behind an Al_2O_3-Nb_2O_5 rich amorphous phase, the composition of which will depend in the local proximity of Al_2O_3 impurities. These observations suggest that not only thermal gradients are responsible for local melting during water assisted FLASH, but also contaminations are segregated at grain boundaries, producing low melting point secondary phases that promote densification and sliding.

To explain the formation of the alumina-niobia formation at GBs, the respective phase diagram for those phases is shown in Figure 9 [30]. Above ~40 mol% Al_2O_3, a liquid phase is present at T > ~1200 ºC. This liquid phase persists with a series of eutectic points until there is a slight increase in melting temperature for 100 % Nb_2O_5, confirming that the presence of contaminations as alumina in KNN water assisted FLASH sintering might contribute to grain boundary melting and pore filling with amorphous phases.

We propose therefore that, despite the FLASH furnace temperature not exceeding 300 ºC, the local temperature through Joule heating exceeds 1000 ºC and is sufficient to locally melt grain boundaries. These results are broadly in agreement with Uehashi et al. who FLASH sintered $BaTiO_3$ at 1020 ºC, with an electric field of 100 $V.cm^{-1}$. They reported that GBs partially melted along with BaO volatilisation and accompanied by the formation of a Ba deficient phase, $BaTi_4O_9$ [31].

From the TEM observations we conclude that: i) there is evaporation of Na at the GBs, ii) liquid phase forms at the grain boundaries and iii) bulk KNN retains its stoichiometry and structure.

FEM (Finite Element Modelling) of the current distribution during FLASH sintering was also performed. We consider only the effect that the geometry has upon the joule heating effect. We first consider the possible geometric points of contact between the particles. Each simulated model combined two interacting 0.5 µm size cubes, overlapped by 50 nm and generating a connection point. The cubes were orientated in three directions to provide different geometric configurations: face-face, (100)-(100), edge-face, (100)-(110), face to vertex, (100)-(111) and vertex to vertex direction, where the cubes are aligned in the (111)-(111) direction as shown in figure 10. Each cube is assigned the electrical properties (conductivity) of KNN [32].

Each configuration was meshed and a refinement applied at the connection point to ensure convergence. It is important to note that the goal of the FEM model is to explain the possible particle penetration, and the possible relation between particle contact and generated heat by FLASH sintering. More complex and accurate modelling work is now being conducted.

To perform this FEM calculations, a potential difference was applied over the cubes, such that the current was forced through the contact points. To calibrate the voltage and provide a value to allow comparison, the face to face configuration as shown in figures 10 (a, b) was used. An applied voltage of 0.08 V gave rise to a maximum current density of 60 $mA.mm^{-2}$ in the model, consistent with current limited values and generating Joule heating of 3.6 $kW.mm^{-3}$. To ensure similarity between the models, the same voltage was then used to highlight the increase in current density and associated Joule heating that would arise due to changes in the geometry of particle to particle contact. It should be noted that the approach of maintaining this voltage may lead to unreasonable current densities and heating effects, as the material may melt before this voltage could be reached. The absolute values are thus not as important as the comparison between them. A line-scan was used through the centre of the model to extract these values as a function of distance from the connection point, and the results are shown in figure 11.

When the cuboid particles were orientated face-edge, the current density increased by a factor of two, to 120 $mA.mm^{-2}$, figure 11 (a). The associated Joule heating, due to its dependence on the square of the current, rises to 14 $kW.mm^{-3}$. Values of 282 $mA.mm^{-2}$ and 455 $mA.mm^{-2}$ are measured for the face to vertex and vertex to vertex models, respectively, accompanied by Joule heating with a face-vertex and vertex-vertex configuration of 70 $kW.mm^{-3}$ and 200 $kW.mm^{-3}$, respectively.

Asymmetry was also observed in models in which two different orientations of cubes are used. For face-edge and face-vertex configurations, greater Joule heating is measured in the edge or vertex-oriented cube with deeper penetration. The asymmetry can be attributed to the initialisation of the model set-up and overlap of the cubes. As the model does not simulate the evolution of this process, this aspect is a subject for further work and analysis.

The maximum value of the vertex-vertex system was greater than those measured from the central line-scan. Joule heating was found to be significantly higher on the outer surface of the cube, around the connection point, figure 10(g), than through the centre, figure 11. Current densities in excess of 1000 $mA.mm^{-2}$ occurred at the surface, corresponding to a Joule heating effect of over 1000 $kW.mm^{-3}$, 16x and 250x, respectively, greater that the face-face configuration. Although physical these values would not be possible, we propose that this significant increase in heating arising from the orientation of the cube quickly would lead to fast thermal runaway during FLASH sintering, resulting in a larger local concentration of liquid phase at these points than others.

The SEM and TEM evidence combined with FEM, clearly indicate that joule heating is a major factor in densification. The channelling of current along open porosity emphasises the importance of adsorbed water and the cuboid shape of KNN particles highlights the role of contact geometry on current density and local heating. The formation of liquid phase (residual amorphous regions at the GB) occurs often in the presence of impurities. Although a liquid phase at high temperature will enhance diffusion, the large volume fraction of liquid suggests that densification is also driven by minimisation of surface energy of the liquid phase, enabled by sliding of grain

boundaries. The work demonstrates the need for further research on the role of particle geometry and size and impurities in water assisted FLASH sintering.

Conclusion

This work describes for the first time the mechanism of low-temperature water assisted FLASH sintering in complex oxides such as KNN and establishes the relation between the geometry of particle contact and local Joule heating. Our observations suggest that conventional diffusion and mass transport at GBs is not solely responsible for the densification of KNN. We postulate that densification occurs through current channelling along open pores made more conductive by the adsorption of water onto the particle surface. We attribute densification to the sliding of grain boundaries and viscous flow of the liquid phase generated from melting, driven by minimisation of surface energy. We note that our work demonstrates for the first time the densification of a lead-free piezoceramic using water assisted FLASH sintering and thus has ramifications not only for materials substitution but more generally for the reduction of carbon consumption in the ceramics industry.

AUTHOR INFORMATION

Corresponding Author

*Paula M. Vilarinho, email: paula.vilarinho@ua.pt

Acknowledgments

This work is financed by Portugal 2020 through European Regional Development Fund (ERDF), in the frame of Operational Competitiveness and Internationalization Programme (POCI), in the scope of the project “FLASH sintering of lead free functional

oxides towards sustainable processing of materials for energy and related applications- FLASH", POCI-01-0247-FEDER-029078. This work was developed within the scope of the project CICECO-Aveiro Institute of Materials, FCT Ref. UID/CTM/50011/2019, financed by national funds through the FCT/MCTES. Ricardo Serrazina acknowledges FCT for financial support (SFRH/PD/BD/128411/2017). Dr J. S. Dean and Professor I. M. Reaney acknowledge the support of EPSRC grants (EP/L017563/1 and EP/P019919/1).

References

[1] S. Chu, Y. Cui, and N. Liu, "The path towards sustainable energy," Nat. Mater., vol. 16, no. 1, pp. 16–22, 2016.

[2] E. Manavalan and K. Jayakrishna, "A review of Internet of Things (IoT) embedded sustainable supply chain for industry 4.0 requirements," Comput. Ind. Eng., vol. 127, no. November 2018, pp. 925–953, 2018.

[3] M. Cologna, B. Rashkova, and R. Raj, "Flash Sintering of Nanograin Zirconia in <5 s at 850°C," J. Am. Ceram. Soc., vol. 93, no. 11, pp. 3556–3559, 2010.

[4] M. Yu, S. Grasso, R. Mckinnon, T. Saunders, and M. J. Reece, "Review of flash sintering: materials, mechanisms and modelling," Adv. Appl. Ceram., vol. 116, no. 1, pp. 24–60, 2017.

[5] C. E. J. Dancer, "Flash sintering of ceramic materials," Mater. Res. Express, vol. 3, no. 10, 2016.

[6] J. Nie, Y. Zhang, J. M. Chan, R. Huang, and J. Luo, "Water-assisted flash sintering: Flashing ZnO at room temperature to achieve ~ 98% density in seconds," Scr. Mater., vol. 142, pp. 79–82, 2018.

[7] J. F. Li, K. Wang, F. Y. Zhu, L. Q. Cheng, and F. Z. Yao, "(K, Na) NbO_3-based

lead-free piezoceramics: Fundamental aspects, processing technologies, and remaining challenges," J. Am. Ceram. Soc., vol. 96, no. 12, pp. 3677–3696, 2013.

[8] C.-H. Hong et al., "Lead-free piezoceramics and Where to move on?," J Mater., vol. 2, pp. 1–24, 2016.

[9] H. Birol, D. Damjanovic, and N. Setter, "Preparation and characterization of ($K_{0.5}Na_{0.5}$) NbO_3 ceramics," J. Eur. Ceram. Soc., vol. 26, no. 6, pp. 861–866, 2006.

[10] M. A. Rafiq, A. Tkach, M. E. Costa, and P. M. Vilarinho, "Defects and charge transport in Mn-doped $K_{0.5}Na_{0.5}NbO_3$ ceramics," Phys. Chem. Chem. Phys., vol. 17, no. 37, pp. 24403–24411, 2015.

[11] G. Corapcioglu, M. A. Gulgun, K. Kisslinger, S. Sturm, S. K. Jha, and R. Raj, "Microstructure and microchemistry of flash sintered $K_{0.5}Na_{0.5}NbO_3$," J. Ceram. Soc. Japan, vol. 124, no. 4, pp. 321–328, 2016.

[12] W. Ji, B. Parker, S. Falco, J. Y. Zhang, Z. Y. Fu, and R. I. Todd, "Ultra-fast firing: Effect of heating rate on sintering of 3YSZ, with and without an electric field," J. Eur. Ceram. Soc., vol. 37, no. 6, pp. 2547–2551, 2017.

[13] Y. Zhang, J. Nie, J. M. Chan, and J. Luo, "Probing the densification mechanisms during flash sintering of ZnO," Acta Mater., vol. 125, pp. 465–475, 2017.

[14] W. D. Kaplan, D. Chatain, P. Wynblatt, and W. C. Carter, "A review of wetting versus adsorption, complexions, and related phenomena: The rosetta stone of wetting," J. Mater. Sci., vol. 48, no. 17, pp. 5681–5717, 2013.

[15] P. R. Cantwell, M. Tang, S. J. Dillon, J. Luo, G. S. Rohrer, and M. P. Harmer, "Grain boundary complexions," Acta Mater., vol. 62, no. 1, pp. 1–48, 2014.

[16] J. Luo, "The scientific questions and technological opportunities of flash

sintering: From a case study of ZnO to other ceramics," Scr. Mater., vol. 146, pp. 260–266, 2018.

[17] M. Jiang et al., "Seed-Free Solid-State Growth of Large Lead-Free Piezoelectric Single Crystals: (Na<inf>1/2</inf>K<inf>1/2</inf>)NbO<inf>3</inf>," J. Am. Ceram. Soc., vol. 98, no. 10, pp. 2988–2996, 2015.

[18] R. Raj, M. Cologna, and J. S. C. Francis, "Influence of externally imposed and internally generated electrical fields on grain growth, diffusional creep, sintering and related phenomena in ceramics," J. Am. Ceram. Soc., vol. 94, no. 7, pp. 1941–1965, 2011.

[19] J. S. C. Francis, M. Cologna, D. Montinaro, and R. Raj, "Flash sintering of anode-electrolyte multilayers for SOFC applications," J. Am. Ceram. Soc., vol. 96, no. 5, pp. 1352–1354, 2013.

[20] D. Sohrabi Baba Heidary, M. Lanagan, and C. A. Randall, "Contrasting energy efficiency in various ceramic sintering processes," J. Eur. Ceram. Soc., vol. 10, no. October, 2017.

[21] M. Biesuz, D. Rizzi, and V. M. Sglavo, "Electric current effect during the early stages of field-assisted sintering," J. Am. Ceram. Soc., no. April, pp. 1–10, 2018.

[22] W. Qin, H. Majidi, J. Yun, and K. van Benthem, "Electrode Effects on Microstructure Formation During FLASH Sintering of Yttrium-Stabilized Zirconia," J. Am. Ceram. Soc., vol. 99, no. 7, pp. 2253–2259, 2016.

[23] K. S. Naik, V. M. Sglavo, and R. Raj, "Flash sintering as a nucleation phenomenon and a model thereof," J. Eur. Ceram. Soc., vol. 34, no. 15, pp. 4063–4067, 2014.

[24] S. Zhang, H. J. Lee, C. Ma, and X. Tan, "Sintering Effect on Microstructure and Properties of (K,Na)NbO_3 Ceramics," J. Am. Ceram. Soc., vol. 94, no. 11, pp.

3659–3665, 2011.

[25] J. Narayan, “A new mechanism for field-assisted processing and flash sintering of materials,” Scr. Mater., vol. 69, no. 2, pp. 107–111, 2013.

[26] J. Narayan, “Grain growth model for electric field-assisted processing and flash sintering of materials,” Scr. Mater., vol. 68, no. 10, pp. 785–788, 2013.

[27] B. Malič et al., “Sintering of lead-free piezoelectric sodium potassium niobate ceramics,” Materials (Basel)., vol. 8, no. 12, pp. 8117–8146, 2015.

[28] R. Chaim, “Particle surface softening as universal behaviour during flash sintering of oxide nano-powders,” Materials (Basel)., vol. 10, no. 2, 2017.

[29] R. Chaim, G. Chevallier, A. Weibel, and C. Estournès, “Flash sintering of dielectric nanoparticles as a percolation phenomenon through a softened film,” J. Appl. Phys., vol. 121, no. 14, 2017.

[30] R. S. Roth, T. Negas, and L. P. Cook, Phase diagrams for ceramists, 1st edition. The American Ceramic Society, 1981.

[31] A. Uehashi, K. Sasaki, T. Tokunaga, H. Yoshida, and T. Yamamoto, “Formation of secondary phase at grain boundary of flash-sintered $BaTiO_3$,” Microscopy, vol. 63, no. suppl 1, pp. i18–i19, 2014.

[32] K. Singh, V. Lingwal, S. C. Bhatt, and N. S. Panwar, “Dielectric properties of potassium sodium niobate mixed system,” Mater. Res. Bull., vol. 36, pp. 2365–2374, 2001.

FIGURES CAPTIONS

Figure 1 – Schematic of the FLASH sintering setup used in this work. The specimen is parallelepiped shaped and is placed in between two platinum electrodes. The electrodes are connected to platinum wires and those to the power source. One of the electrodes is fixed by an alumina part and the second one is free to move to follow the shrinkage of the specimen, trough the movement of an external alumina stub.

Figure 2 – XRD patterns for powder and low-temperature FLASH sintered. Indexed with PDF file number 01-084-6855.

Figure 3a) – SEM micrographs of KNN green pellet and b) FLASH sintered KNN. c) is a low magnification of FLASH sintered KNN showing current channelling.

Figure 4 – TEM micrograph of several grains in FLASH sintered KNN. The orange arrows indicate the particle movement and the green circles the amorphized phase that is filling some pores.

Figure 5 – TEM micrograph exemplifying the consolidation by FLASH of two particles with face-face [(100)-(100)] contact.

Figure 6 – TEM micrograph exemplifying vertex-face configuration. The possible original particle shape is outlined and the amorphous phase arrowed.

Figure 7 – (a) Local melting of the FLASH sintered KNN grain boundary and pore filling with amorphous phase. The star symbol indicates the representative local for diffraction patterns of crystalline area (with a 110 zone axis), while the circle stands

for amorphous areas. (b) and (c) show the respective diffraction patterns for crystalline and amorphous areas.

Figure 8 – EDS spectra for FLASH sintered KNN grain (grey) and GB (blue).

Figure 9 – Al_2O_3 – Nb_2O_5 phase diagram. [30]

Figure 10 – The simulated current densities (a,c,e,g) and Joule heating (b,d,f,h) arising from face-face (a,b), face-edge(c,d), face-vertex(e,f) and vertex-vertex(g,h) contacts within a green KNN body. Note a logarithmic scale is used to plot the Joule heating effect.

Figure 11. The current density (a) and Joule heating (b) profiles taken from line scans through the centre of the model. These are plotted as a function of the distance of the connection point (i.e. where the cubes overlap).

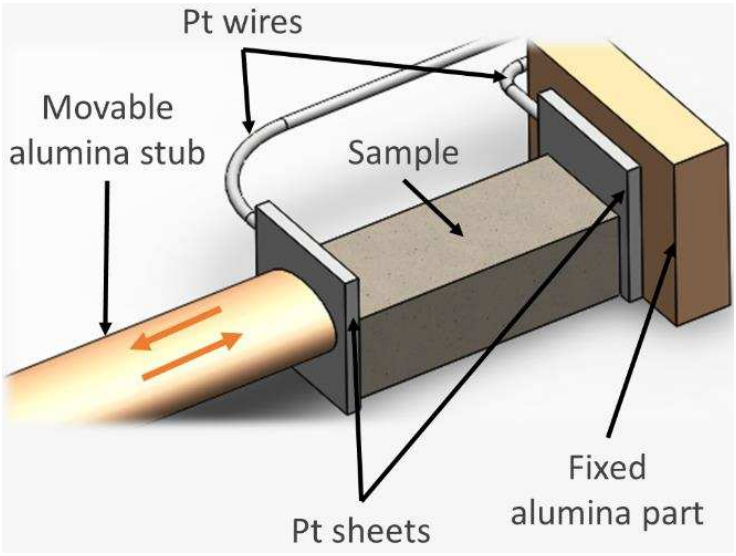

Figure 2 – Schematic of the FLASH sintering setup used in this work. The specimen is parallelepiped shaped and is placed in between two platinum electrodes. The electrodes are connected to platinum wires and those to the power source. One of the electrodes is fixed by an alumina part and the second one is free to move to follow the shrinkage of the specimen, trough the movement of an external alumina stub.

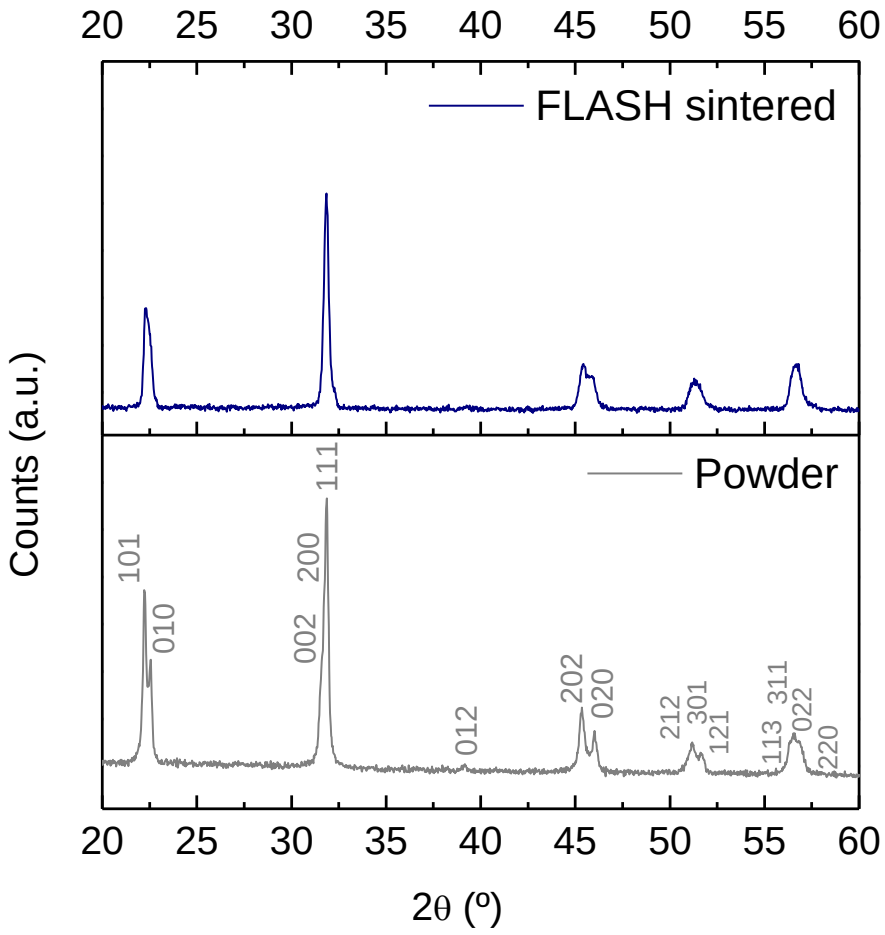

Figure 2 – XRD patterns for powder and low-temperature FLASH sintered. Indexed with PDF file number 01-084-6855.

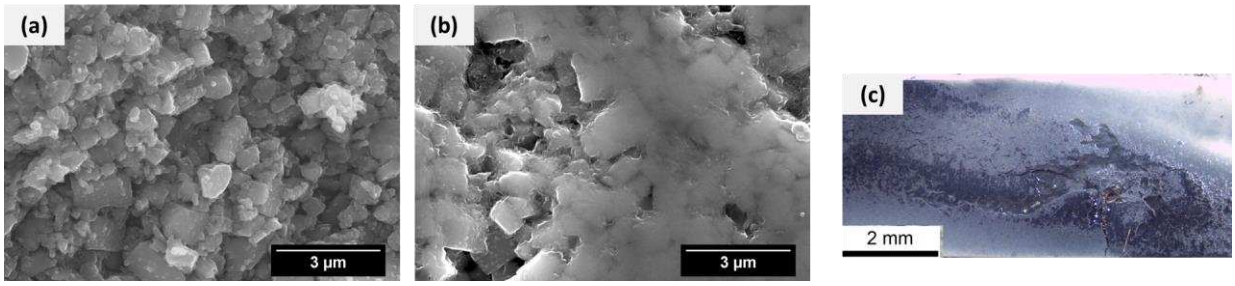

Figure 3a) – SEM micrographs of KNN green pellet and b) FLASH sintered KNN. c) is a low magnification of FLASH sintered KNN showing current channelling.

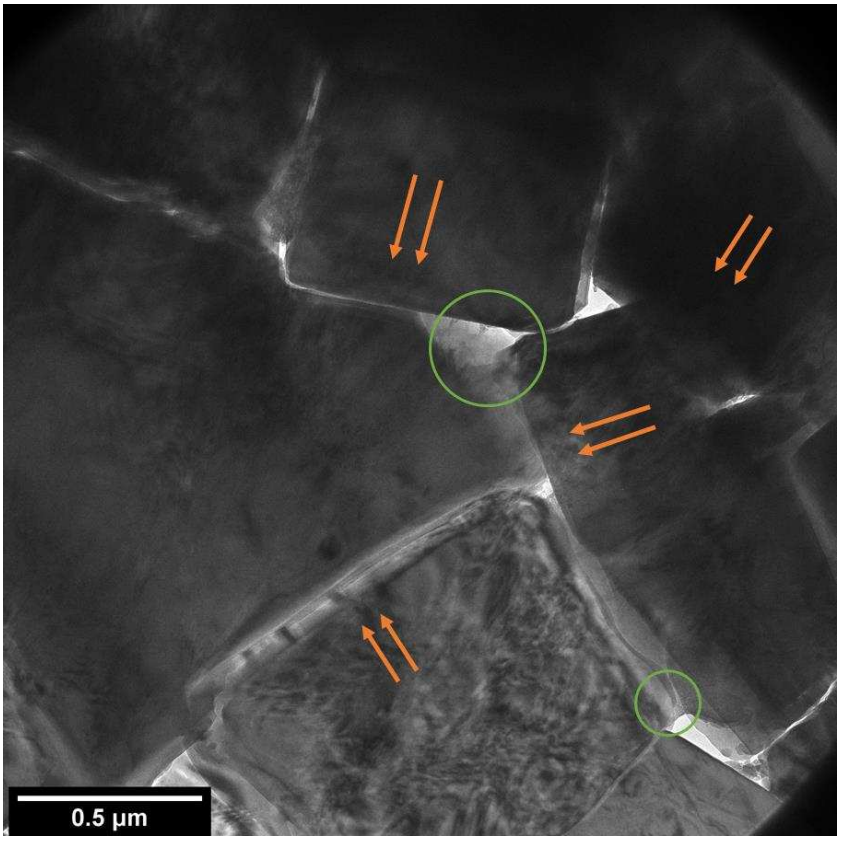

Figure 4 – TEM micrograph of several grains in FLASH sintered KNN. The orange arrows indicate the particle movement and the green circles the amorphized phase that is filling some pores.

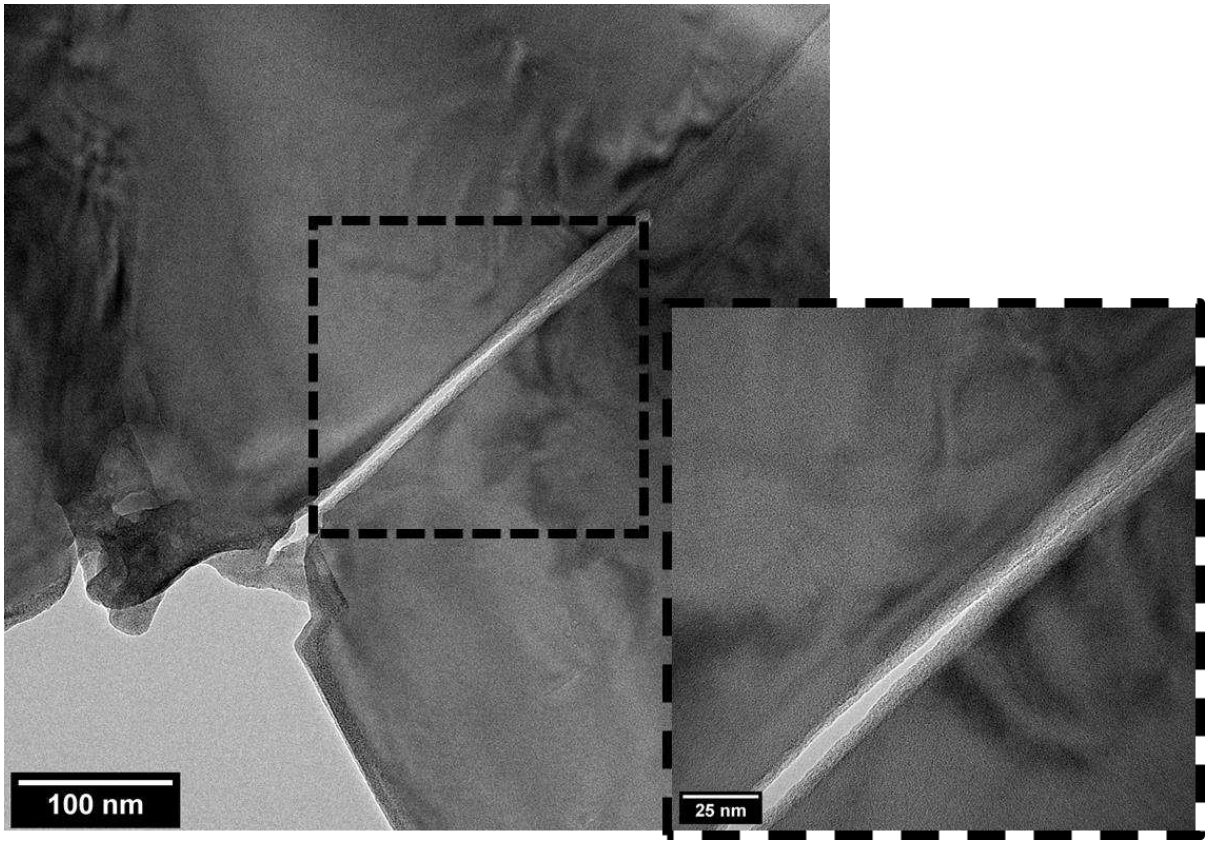

Figure 5 – TEM micrograph exemplifying the consolidation by FLASH of two particles with face-face [(100)-(100)] contact.

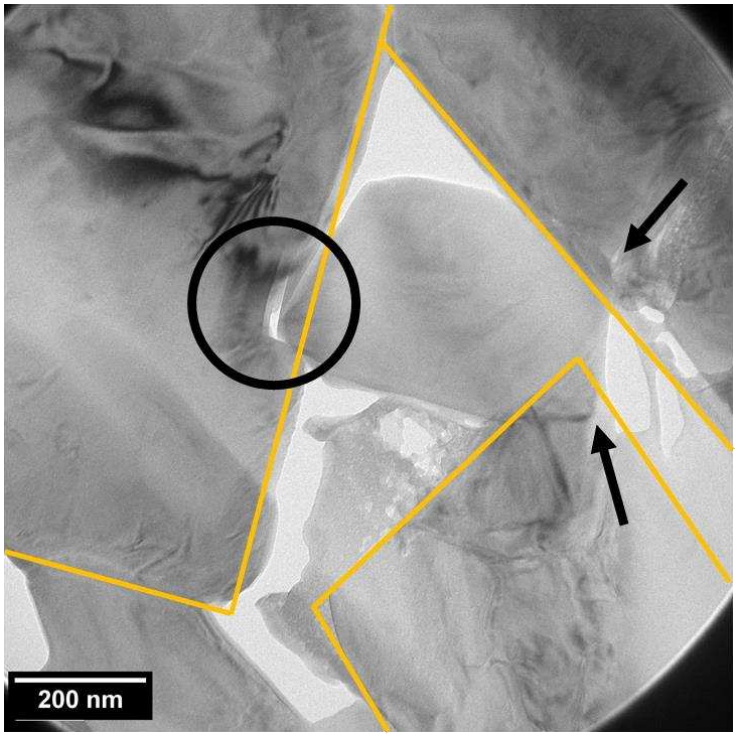

Figure 6 – TEM micrograph exemplifying vertex-face configuration. The possible original particle shape is outlined and the amorphous phase arrowed.

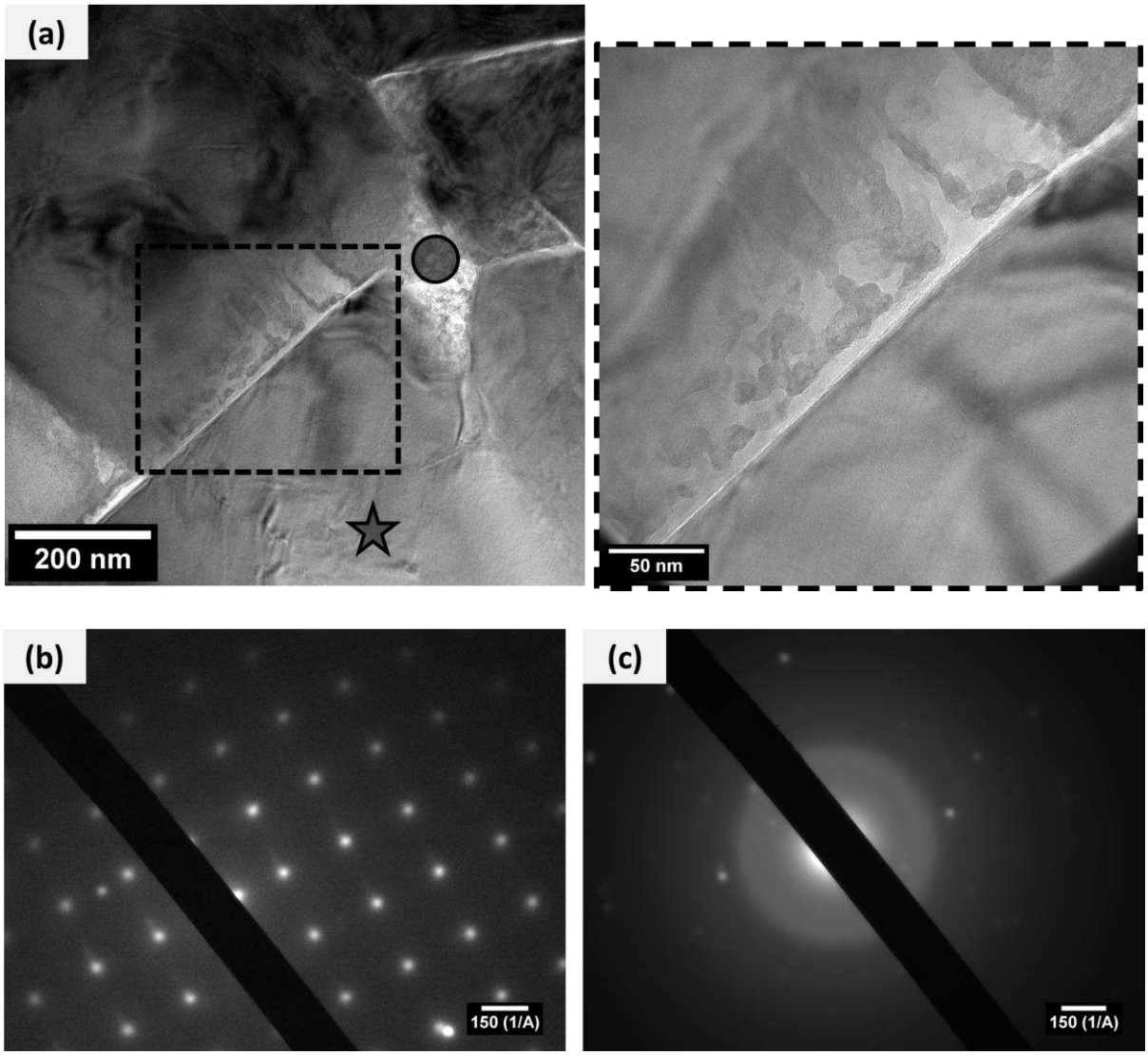

Figure 7 – (a) Local melting of the FLASH sintered KNN grain boundary and pore filling with amorphous phase. The star symbol indicates the representative local for diffraction patterns of crystalline area (with a 110 zone axis), while the circle stands for amorphous areas. (b) and (c) show the respective diffraction patterns for crystalline and amorphous areas.

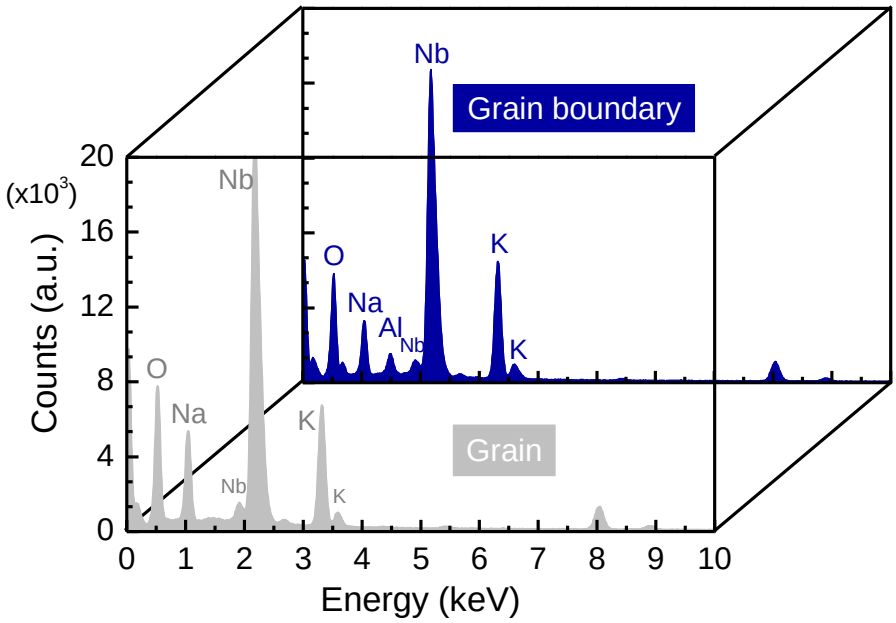

Figure 8 – EDS spectra for FLASH sintered KNN grain (grey) and GB (blue).

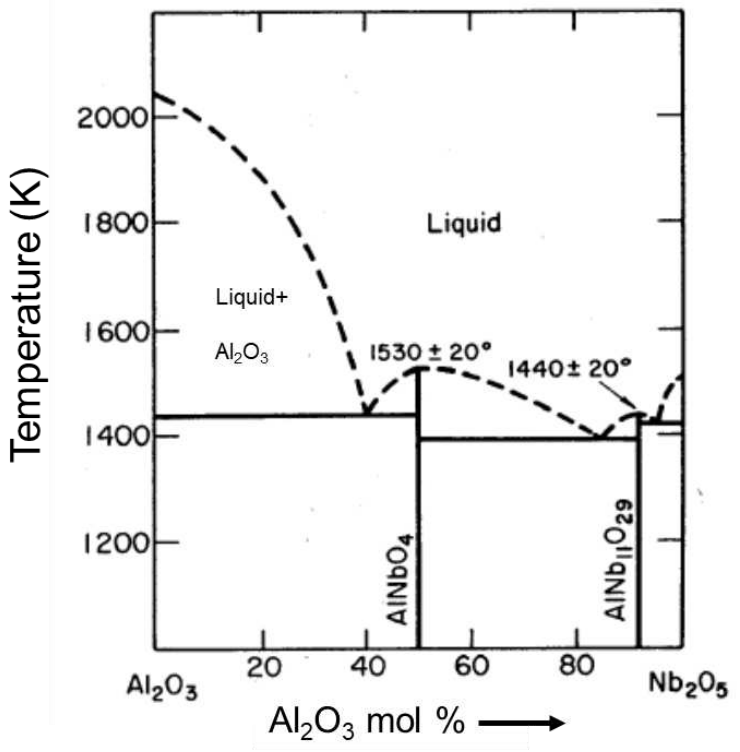

Figure 9 – Al_2O_3 – Nb_2O_5 phase diagram. [30]

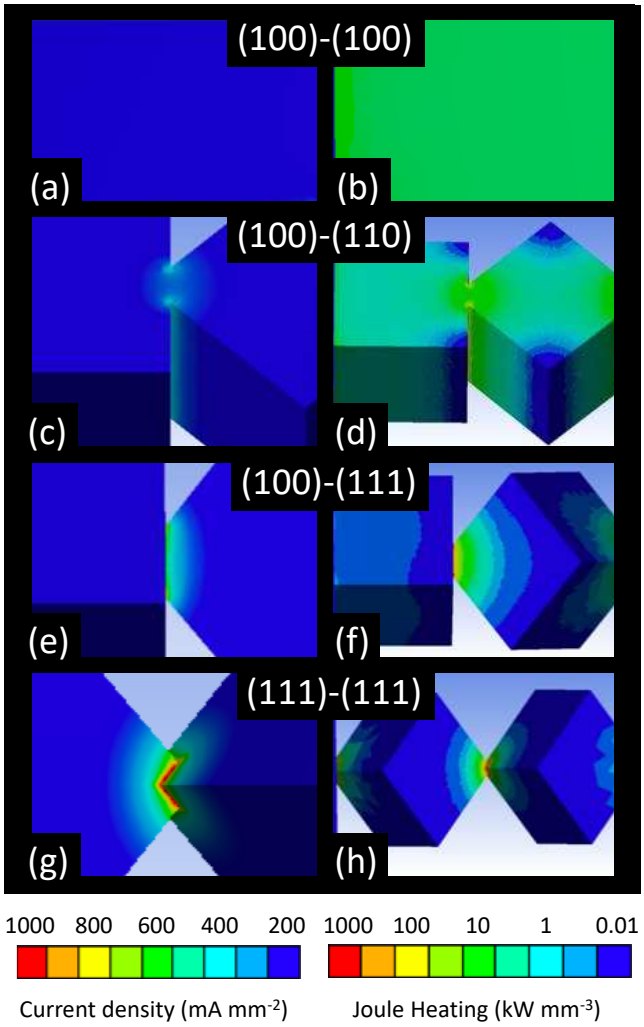

Figure 10 – The simulated current densities (a,c,e,g) and Joule heating (b,d,f,h) arising from face-face (a,b), face-edge(c,d), face-vertex(e,f) and vertex-vertex(g,h) contacts within a green KNN body. Note a logarithmic scale is used to plot the Joule heating effect.

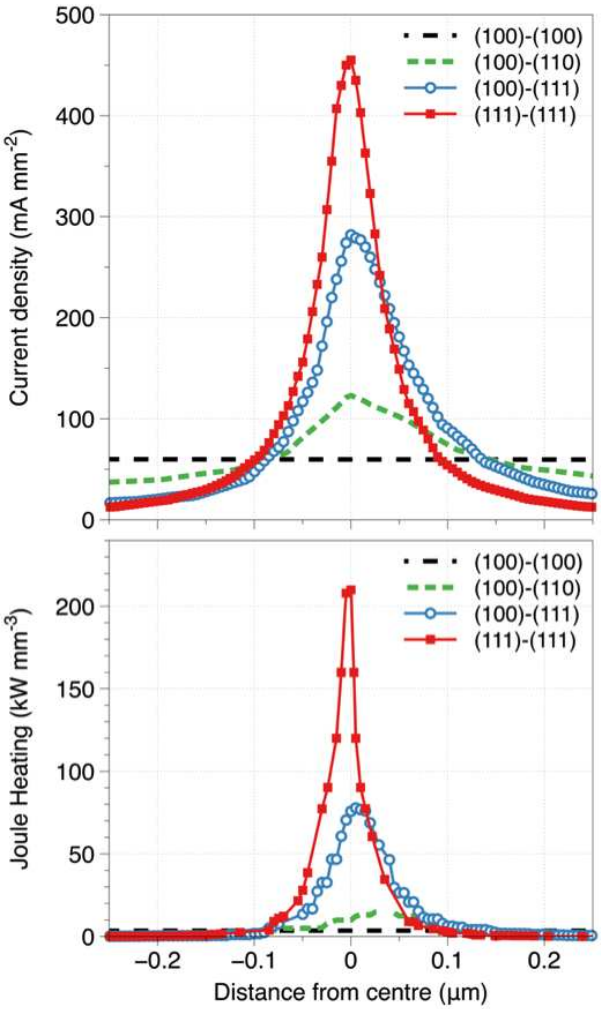

Figure 11. The current density (a) and Joule heating (b) profiles taken from line scans through the centre of the model. These are plotted as a function of the distance of the connection point (i.e. where the cubes overlap).